Electronic Supplementary Information for "The role of temperature in the rigidity-controlled fracture of elastic networks"

Justin Tauber, Aimée R. Kok, Jasper van der Gucht,* and Simone Dussi

Dependence of non-affinity on the reference coordinates

We calculate the non-affine deformation with respect to the time averaged position at 0% strain (Fig. S1(a)) $\overline{\mathbf{r}}_0$. Alternatively, the non-affinity can be calculated with respect to the initial positions of the nodes (located on a regular triangular lattice) $\mathbf{r}_{\text{init}}$ (Fig. S1(b)). The difference between Fig. S1(a) and Fig. S1(b) indicates that temperature has an effect on the equilibrium node positions at 0% strain. This is in contrast with athermal networks and bending stabilized networks, where the equilibrium node positions are equal to the initial position of the nodes. Fig. S1(c) shows that the average displacement of the nodes from their initial position to their equilibrium position $dr = \langle|\overline{\mathbf{r}}_0 - \mathbf{r}_{\text{init}}|\rangle$ depends on both temperature and connectivity. Especially below the isostatic point there are significant reorganizations within the network. However, at high temperatures also the network structure well above the isostatic point is affected. Clearly, the thermal fluctuations do affect the equilibrium structure at 0% strain.

Size of the thermal fluctuations

To quantify the size of the thermal fluctuations, we monitor the root mean squared displacement of the nodes with respect to their equilibrium position $\sqrt{\langle \mathbf{u}^2_{\text{therm}} \rangle}$ and define the size of the fluctuations as $dr_{\text{fluc}} = \sqrt{\overline{\langle \mathbf{u}^2_{\text{therm}} \rangle}}$ with $\overline{\cdot}$ representing a time-average. From Fig. S2(a) it is clear that the size of the fluctuations of the nodes depends on both temperature and connectivity. In general the size of the fluctuations decreases with an increase in connectivity, indicating there is feedback between the number of constraints imposed on a node in the network and how far the nodes can move. Before measuring $\sqrt{\overline{\langle \mathbf{u}^2_{\text{therm}} \rangle}}$, all systems are subjected to the same calibration run of 100τ (see Fig. S2(b)/(c)). We note that for $p = 0.65$ (Fig. S2(b)) the required time to reach a stable value of $\sqrt{\overline{\langle \mathbf{u}^2_{\text{therm}} \rangle}}$ is longer for lower temperatures, indicating that the rate of equilibration depends on temperature. Furthermore, we see that at the higher connectivity value $p = 0.90$ (Fig. 2(c)) the fluctuations are smaller and reach their equilibrium value faster.

Relation between time-averaged non-affinity and instantaneous non-affinity

In an athermal elastic network the position of the crosslinks is determined by the applied deformation and the non-affine response of the nodes. In a thermal elastic network, the positions of the nodes are also influenced by thermal fluctuations of the nodes. The position of a node $\mathbf{r}$ under uniaxial extension ε can therefore be described as

$$\mathbf{r}(\varepsilon, T, p) = \overline{\mathbf{r}}_0 + \mathbf{u}_{\text{aff}}(\varepsilon) + \mathbf{u}_{\text{naff}}(\varepsilon, T, p) + \mathbf{u}_{\text{therm}}(\varepsilon, T, p) \ , \tag{1}$$

where p is the network connectivity parameter, and T temperature. $\mathbf{u}$ stands for a displacement vector and $\overline{\mathbf{r}}_0$ is the time averaged position at 0% strain. If a system is fixed at a certain strain ε the average position of the particle over time will be,

$$\overline{\mathbf{r}} = \overline{\mathbf{r}}_0 + \mathbf{u}_{\text{aff}}(\varepsilon) + \mathbf{u}_{\text{naff}}(\varepsilon, T, p) \ , \tag{2}$$

assuming $|\overline{\mathbf{u}}_{\text{therm}}| = 0$. If we instead monitor the average size of the fluctuations of the nodes we find that

$$\overline{(\mathbf{r} - \overline{\mathbf{r}})^2} = \mathbf{u}^2_{\text{therm}}(\varepsilon, T, p) \ . \tag{3}$$

Note that in case of drift in the system center of mass, this needs to be taken into account. In our case, we assume $< \mathbf{r} >= \mathbf{r}_{\text{com}}$. Below, we will detail how these contributions are related to the measure for non-affinity Γ.

Non-affine response of time averaged positions

We will start with the non-affinity based on time-averaged positions (Eq. 2), as this parameter is directly related to the non-affinity parameter discussed for athermal systems that describes the size of non-affine rearrangements of the network.

$$\Gamma_{\text{mech}} = \frac{\langle(\overline{\mathbf{r}}-\overline{\mathbf{r}}_{\text{aff}})^2\rangle}{\varepsilon^2\ell_0^2} = \frac{\langle(\mathbf{u}_{\text{naff}})^2\rangle}{\varepsilon^2\ell_0^2} \quad . \tag{4}$$

To simplify the equation our definition for $\overline{\mathbf{r}}$ is used (Eq. 2) and the definition $\overline{\mathbf{r}}_{\text{aff}} = \overline{\mathbf{r}}_0 + \mathbf{u}_{\text{aff}}$.

Non-affine response of instantaneous positions

In a system with thermal fluctuations, the instantaneous positions of the node will also be determined by (non-affine) thermal fluctuations (See Eq. 1). While monitoring the non-affinity during a continuous deformation, the non-affinity parameter Γ will therefore include both the effects of non-affine rearrangements and thermal fluctuations.

$$\Gamma = \frac{\langle(\mathbf{r}-\overline{\mathbf{r}}_{\text{aff}})^2\rangle}{\varepsilon^2\ell_0^2} = \frac{\langle(\mathbf{u}_{\text{naff}}+\mathbf{u}_{\text{therm}})^2\rangle}{\varepsilon^2\ell_0^2} \quad . \tag{5}$$

The relation between Γ and Γ_{mech}

An essential difference with respect to athermal networks is that Γ is a result of both non-affine structural rearrangements and thermal fluctuations. Here we show the relation between Γ_{mech} and Γ. We can rewrite the non-affinity such that we only have sums over all particles on the right hand side.

$$[\Gamma - \Gamma_{\text{mech}}]N\varepsilon^2\ell_0^2 = \sum((\mathbf{u}_{\text{naff}}+\mathbf{u}_{\text{therm}})^2) - \sum((\mathbf{u}_{\text{naff}})^2) = \sum(\mathbf{u}_{\text{therm}}^2 + 2\mathbf{u}_{\text{naff}}\cdot\mathbf{u}_{\text{therm}}) \quad . \tag{6}$$

Returning to the averages over all particles we can now distinguish a term related to thermal fluctuations and a cross-term related to both the non-affine deformation and the thermal fluctuations,

$$\Gamma = \Gamma_{\text{mech}} + \frac{\langle\mathbf{u}_{\text{therm}}^2\rangle}{\varepsilon^2\ell_0^2} + \frac{2\langle\mathbf{u}_{\text{naff}}\cdot\mathbf{u}_{\text{therm}}\rangle}{\varepsilon^2\ell_0^2} \quad . \tag{7}$$

Hence, the contributions of structural rearrangements and thermal fluctuations to Γ can not be decoupled.

The influence of driving and viscosity

The mechanical and failure response can depend on both the driving speed and the friction coefficient of the nodes, i.e., viscosity of the implicit solvent. In Fig. S7 we show how these parameters affect the stress-strain curves around the isostatic point (Fig. S7(a-b)) and far above the isostatic point (Fig. S7(d-e)). An increase in either $\dot{\varepsilon}$ or ζ has a similar effect as both parameters affect the relaxation time of stress in the system. Furthermore the friction coefficient controls the amount of damping in the system, from the underdamped regime at low ζ, where inertia plays a role, to the overdamped (Brownian) regime at high ζ, where the effect of inertia is negligible. In general, an increase in these parameters leads to an increase in ductility. Below the isostatic point, both the pre-peak and post-peak behaviour are affected, while above the isostatic point it is mostly the post peak response. Furthermore, we show the peak stress σ_p as a function of the strain rate for $p = 0.65$ and $p = 0.90$ for a range of ζ and two values of T^*: $1 \cdot 10^{-9}$ (purple) and $1 \cdot 10^{-5}$ (blue). We see that typically the peak stress increases with the strain rate. At a higher strain rate, there is less time for stress relaxation, leading to a more affine response and a higher stress in the system. Similarly, we observe that the peak stress increases with an increase in the friction coefficient, which is also related to the time for stress relaxation $\tau_{\text{relax}} = \zeta/\mu$. In the main text, we set the strain-rate $\dot{\varepsilon} = 0.001$ and the friction coefficient $\zeta = 10$. We can observe that for $p = 0.65$ we are in a regime where the effect of $\dot{\varepsilon}$ and ζ on the peak stress is relatively small. At $p = 0.90$ the effect of the strain rate is bigger, however we do not expect that this affects our conclusions.

Estimate of $E_{\mathbf{therm}}/E_{\mathbf{break}}$ in experimental systems

We introduce the ratio between the thermal energy ($E_{\mathrm{therm}} = k_{\mathrm{B}}T$) and the failure energy of a building block (E_{break}) as a measure for the (network level) temperature sensitivity of the failure response of a network material. We can use the expression $T^*/(\frac{1}{2}\lambda^2)$ to get a rough estimate of $E_{\mathrm{therm}}/E_{\mathrm{break}}$ for an experimental system when we know μ and λ of the individual building blocks. Please note, that this approximation assumes a linear stress-strain response of the building blocks ($E_{break} = \frac{1}{2}\mu(\lambda\ell_0)^2$).

Stiff fibre networks: Collagen

Collagen is a stiff athermal fibre network. The spring constant of a stiff fiber can be defined as $\mu = E_y A/\ell_c = E_y \pi r^2/\ell_c$ with E_y the Youngs Modulus of the fibre, A the cross-section of the fibre, ℓ_c the distance between crosslinks, and r the radius of a a fibre. Here we neglect the fiber bending stiffness, which is expected to have only a minor influence on network fracture [1]. Consequently, T^* of a fibre network can be calculated as

$$T^* = \frac{k_{\mathrm{B}}T}{E_y \pi r^2 \ell_c} \quad . \tag{8}$$

For a collagen network with $E_y = 50$ MPa, $r = 30$ nm and assuming that ℓ_c scales with the mesh size of the network $\ell_c \approx \xi = 2$ μm (Based on Ref. [2]) we find that $T^* = 1.5 \cdot 10^{-8}$ at $T = 298$ K, which falls well into the athermal limit. For a value of $\lambda = 0.15$ [1] we find that $T^*/(\frac{1}{2}\lambda^2) = 1.3 \cdot 10^{-6}$ which also falls well into the athermal limit.

Semiflexible polymer networks: Actin

Actin is regarded as a typical example of a semiflexibe polymer. For a semiflexible polymer, the spring constant is $\mu = 90\kappa\ell_p/\ell^4$ (by linear approximation) [3], with ℓ the contour length of the polymer and ℓ_p its persistence length. Using that $\ell_p = \kappa/k_{\mathrm{B}}T$ and $\ell \approx \ell_c$ we find that $\mu = 90 k_{\mathrm{B}}T\ell_p^2/\ell_c^4$, with κ the bending stiffness, ℓ_p the persistence length, and ℓ_c the distance between crosslinks. Thus the reduced temperature of a semiflexible polymer, like actin, is

$$T^* = \frac{\ell_c^2}{90\ell_p^2} \quad . \tag{9}$$

Furthermore, if we assume that a semiflexible polymer breaks once its thermal fluctuations are pulled out, we can calculate the extensibility as the ratio between contour length and the average end-to-end distance without tension. With $\Delta\ell = \ell^2/(6\ell_p)$ the average contraction of a semiflexible polymer with respect to its contour length without tension [3], $\lambda = \ell/(\ell - \Delta\ell) - 1 = \Delta\ell/(l - \Delta\ell)$. Assuming that $\ell \approx \ell_c$ and $\Delta\ell \ll \ell_c$ we can use the simplified expression $\lambda \approx \ell_c/(6\ell_p)$.

For an actin network with fibers with a persistence length of 17 μm [3] and a distance between crosslinks ℓ_c of roughly 300 nm [4] $T^* = 3.5 \cdot 10^{-6}$ which indicates that the effect of temperature at the network level is negligible (note that at the level of the building blocks temperature does play an important role). For these parameters we find that $\lambda = 0.03$ and that $T^*/(\frac{1}{2}\lambda^2) = 8 \cdot 10^{-3}$, which is in the cross-over regime where the failure response is temperature sensitive.

Flexible polymer networks: Freely jointed chain

Flexible polymers are an example of extremely soft network building blocks. In the case of flexible polymers the elastic response of the building blocks can be described based on the freely jointed chain. By linear approximation the spring constant of a freely jointed chain can be written as $\mu = 3k_{\mathrm{B}}T/(Nb^2)$ with N the number of segments and b the segment length. Thus we find that

$$T^* = \frac{k_{\mathrm{B}}T}{\mu\ell_c^2} = \frac{Nb^2}{3\ell_c^2} = \frac{1}{3} \quad , \tag{10}$$

when we use the average end-to-end distance of the chain as an estimate for the distance between crosslinks $l_c = \sqrt{N}b$. Furthermore, if we assume that the extensibility of the chain scales as the ratio between the contour length of the polymer Nb and the average end-to-end distance l_c, we find $\lambda = \sqrt{N} - 1 \approx \sqrt{N}$. Thus, $T^*/(\frac{1}{2}\lambda^2) \approx 2/(3N)$. For a polymer network with $N = 100$ this results in the estimates $T^* = 0.33$ and $T^*/(\frac{1}{2}\lambda^2) = 7 \cdot 10^{-3}$ i.e. the network level mechanical and failure response are both placed well in the

temperature sensitive regime. However, it should be noted that the strong non-linear response of polymer chains might significantly affect this estimate, especially in the failure regime.

References

[1] Federica Burla, Simone Dussi, Cristina Martinez-Torres, Justin Tauber, Jasper van der Gucht, and Gijsje H. Koenderink. Connectivity and plasticity determine collagen network fracture. *Proceedings of the National Academy of Sciences*, 117(15):201920062, 2020.

[2] Andrew M. Stein, David A. Vader, David A. Weitz, and Leonard M. Sander. The micromechanics of three-dimensional collagen-I gels. *Complexity*, 16(4):22–28, 2011.

[3] Chase P. Broedersz and Fred. C. Mackintosh. Modeling semiflexible polymer networks. *Reviews of Modern Physics*, 86(3):995–1036, 2014.

[4] M. L. Gardel. Elastic Behavior of Cross-Linked and Bundled Actin Networks. *Science*, 1301(2004):1301–1305, 2009.

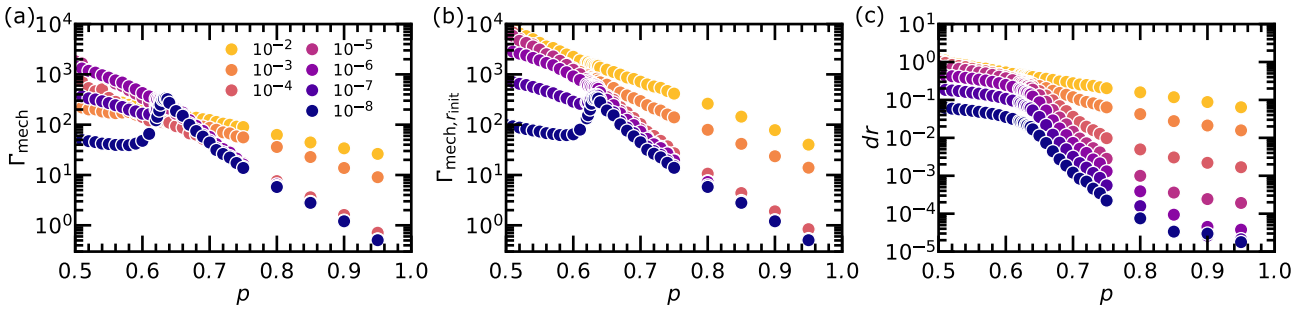

Fig. S1: Non-affine response in the linear regime versus p for a range of T^* (colors are indicated in the legend). (a) The time-averaged (over 1900τ) non-affine response at 1.5% strain with respect to the time-averaged position of the nodes at 0% strain $\bar{\mathbf{r}}_0$. (b) The time-averaged non-affine response at 1.5% strain with respect to the coordinates r_{init} of the initial configuration (a regular triangular lattice). (c) The ensemble averaged displacement $dr = \langle|\bar{\mathbf{r}}_0 - \mathbf{r}_{\mathrm{init}}|\rangle$ at 0% strain. Every data point is based on simulations of at least 10 independent configurations.

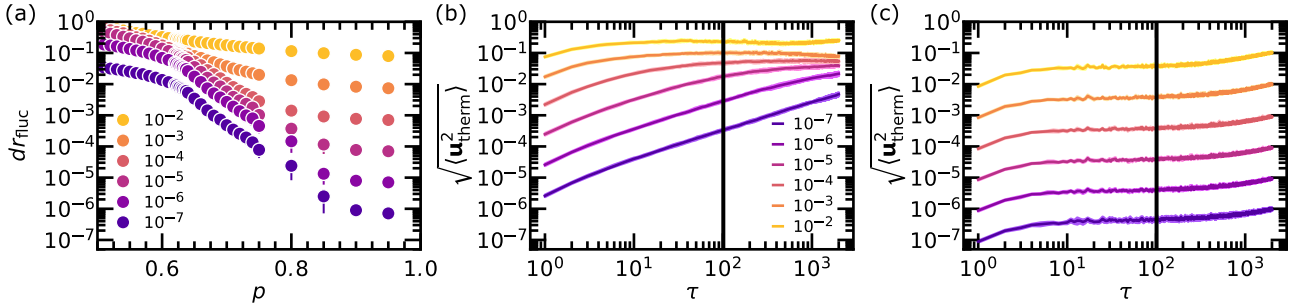

Fig. S2: The size of the thermal fluctuations of the node positions. (a) the time-averaged (over 1900 τ) root mean squared fluctuation size $dr_{\mathrm{fluc}} = \sqrt{\overline{\langle \mathbf{u}^2_{\mathrm{therm}} \rangle}}$ versus p for a range of T^* (colors are indicated in the legend). (b-c) The development of $\sqrt{\langle \mathbf{u}^2_{\mathrm{therm}} \rangle}$ as a function of time (2000 τ in total). The black line is placed at 100 τ, time-averages for Γ_{mech} and $\sqrt{\langle \mathbf{u}^2_{\mathrm{therm}} \rangle}$ are based on data past this line. (b) $p = 0.65$ and (c) $p = 0.90$. Every data point is based on simulations of at least 10 independent configurations.

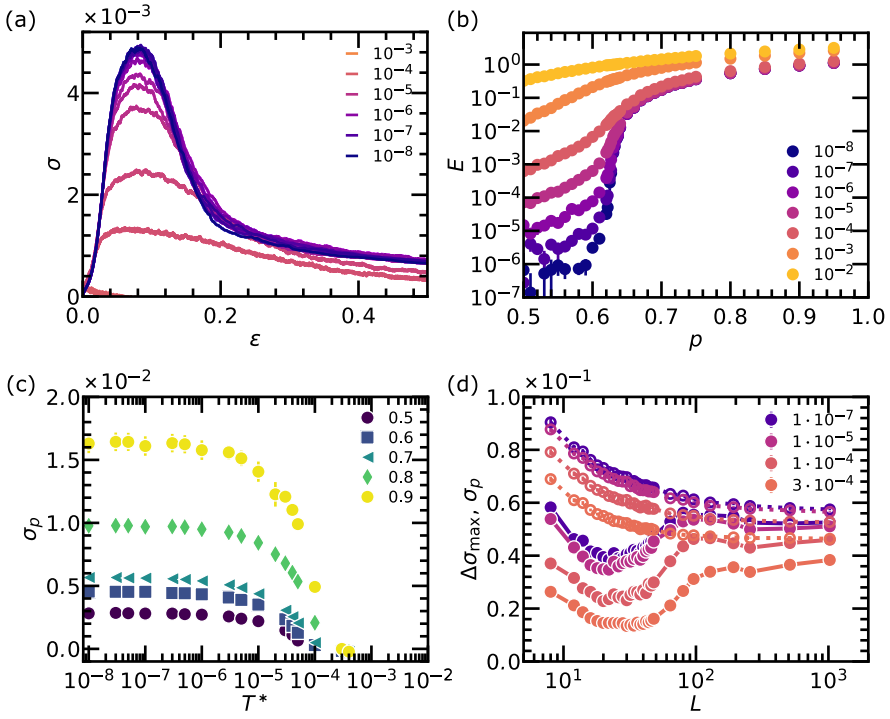

Fig. S3: Main results based on the virial stress including the kinetic component. (a) stress-strain curve for a system with $L = 128$; $p = 0.65$ for a range of reduced temperatures T^* indicated in the legend. Curves are averages over 10 configurations. (b) linear modulus as a function of the dilution factor (p) for a range of T^* (see legend). (c) Peak stress σ_p as a function of the reduced temperature for a range of p (see legend). (d) Maximum stress drop $\Delta\sigma_{max}$ and peak stress σ_p for a networks with $p = 0.80$ as a function of system size L for a range of T^* (see legend).

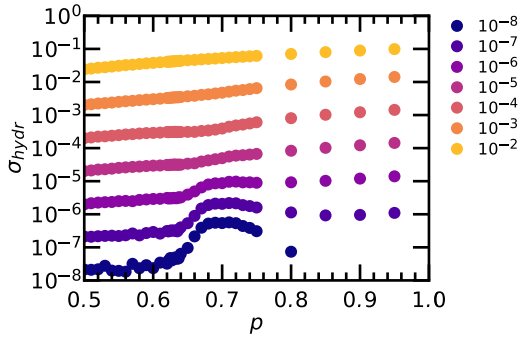

Fig. S4: The time averaged (over 1900 τ) hydrostatic stress at 0% strain as a function of the p for a range of reduced temperatures T^* (see legend). Every data point is based on simulations of at least 10 independent configurations.

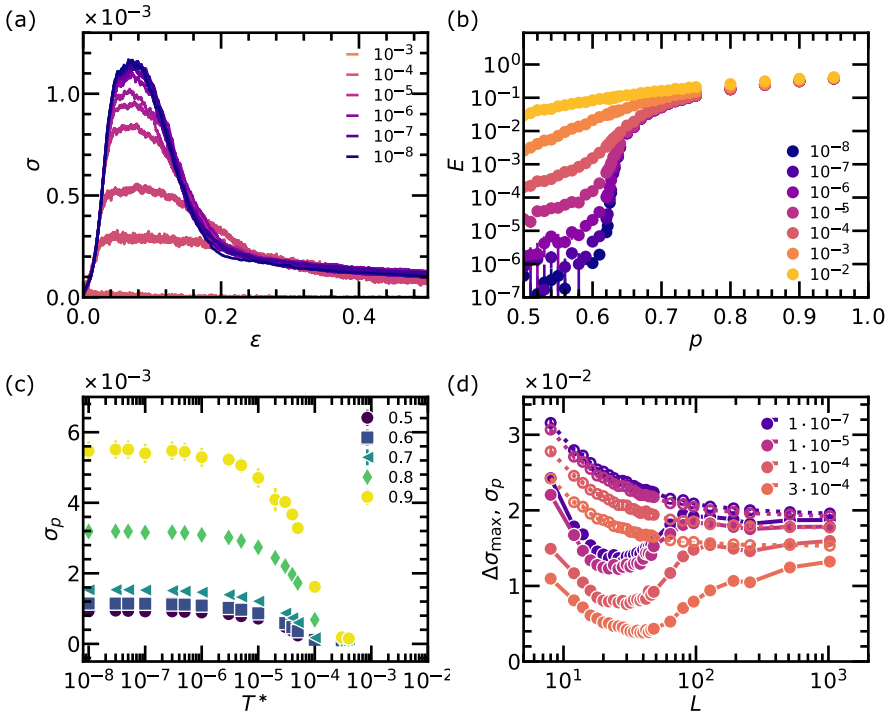

Fig. S5: Main results based on the deviatoric stress $\sigma = \sigma_{yy} - \sigma_{hydr}$. (a) stress-strain curve for a system with $L = 128$; $p = 0.65$ for a range of reduced temperatures T^* indicated in the legend. Curves are averages over 10 configurations. (b) linear modulus as a function of the dilution factor (p) for a range of T^* (see legend). (c) Peak stress σ_p as a function of the reduced temperature for a range of p (see legend). (d) Maximum stress drop $\Delta\sigma_{max}$ and peak stress σ_p for a networks with $p = 0.80$ as a function of system size L for a range of T^* (see legend).

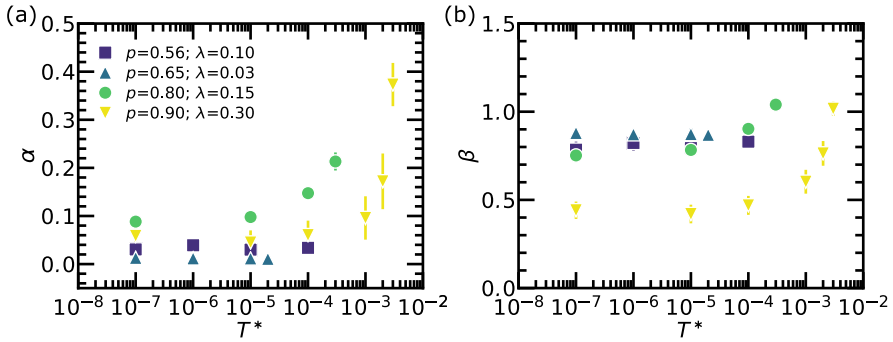

Fig. S6: Fit parameters of the scaling of σ_p with L using the powerlaw $\sigma_p = (L/\alpha)^{-\beta} + \sigma_p^\infty$. σ_p^∞ is reported in the main text. (a) α versus T^*. System parameters are indicated in the legend. (b) β versus T^* for the same systems. Error bars represent the standard error in the fit of α and β, respectively.

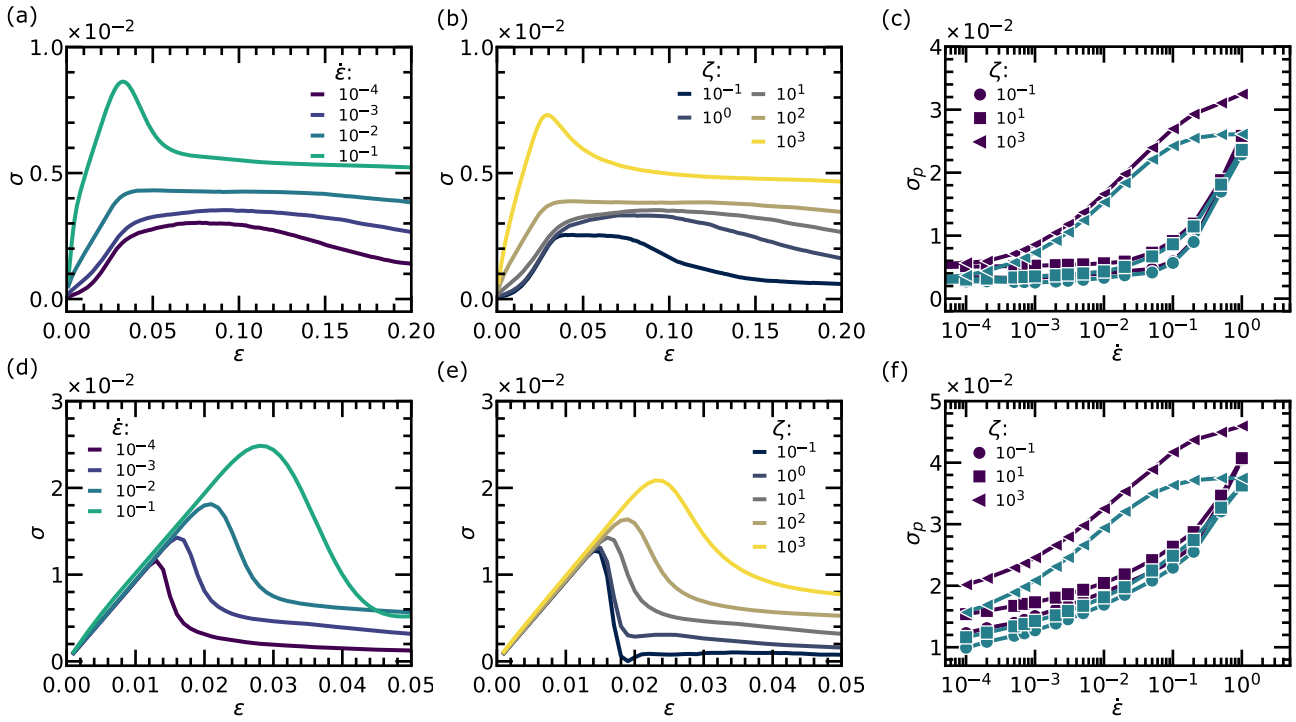

Fig. S7: The influence of driving and friction coefficient on the stress-strain response. (a) Stress versus strain for a network around the isostatic point ($p = 0.65$, $L = 1024$, $\zeta = 10$, $T^* = 1 \cdot 10^{-5}$) for a range of strain rates (see legend). (b) Stress versus strain for a subisostatic network ($p = 0.65$, $L = 1024$, $\dot{\varepsilon} = 0.001$, $T^* = 1 \cdot 10^{-5}$) for a range of ζ (see legend). (c) σ_p versus $\dot{\varepsilon}$ for a networks with $p = 0.65$ and $L = 1024$. σ_p is determined for $T^* = 1 \cdot 10^{-9}$ (purple) and $T^* = 1 \cdot 10^{-5}$ (blue) the shape of the markers indicates the friction coefficient ζ (see legend). Stress versus strain for a network far above the isostatic point ($p = 0.90$, $L = 1024$, $\zeta = 10$, $T^* = 1 \cdot 10^{-5}$) for a range of strain rates (see legend). (e) Stress versus strain for a network far above the isostatic point ($p = 0.90$, $L = 1024$, $\dot{\varepsilon} = 0.001$, $T^* = 1 \cdot 10^{-5}$) for a range of ζ (see legend). (f) σ_p versus $\dot{\varepsilon}$ for networks with $p = 0.90$ and $L = 1024$. Same color code as in (c).

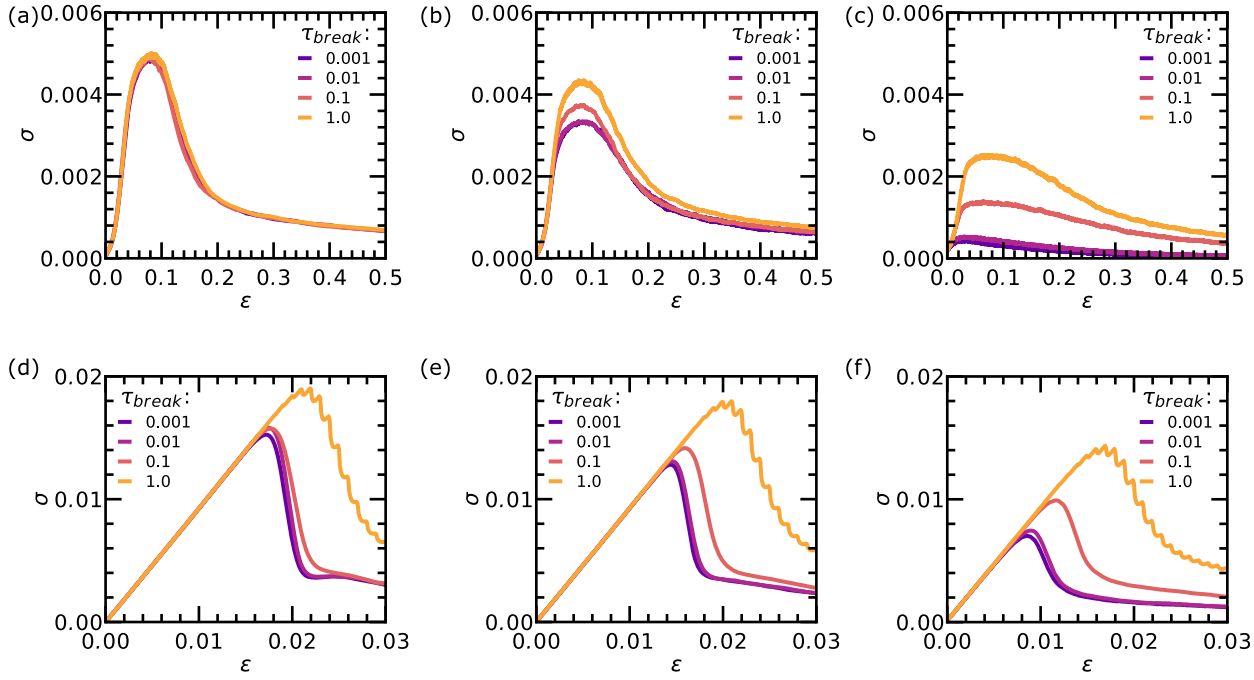

Fig. S8: Effect of bond breaking time τ_{break}, i.e. the time interval between moments when bonds are allowed to rupture, on the stress-strain response. Stress-strain response for a system with $p = 0.65$ and $L = 128$ for a temperature of (a) $T^* = 1 \cdot 10^{-8}$, (b) $T^* = 1 \cdot 10^{-5}$ and (c) $T^* = 5 \cdot 10^{-5}$. Stress-strain response for a system with $p = 0.90$ and $L = 128$ for a temperature of (d) $T^* = 1 \cdot 10^{-8}$, (e) $T^* = 1 \cdot 10^{-5}$ and (f) $T^* = 5 \cdot 10^{-5}$. The curves are averaged over 30 configurations.

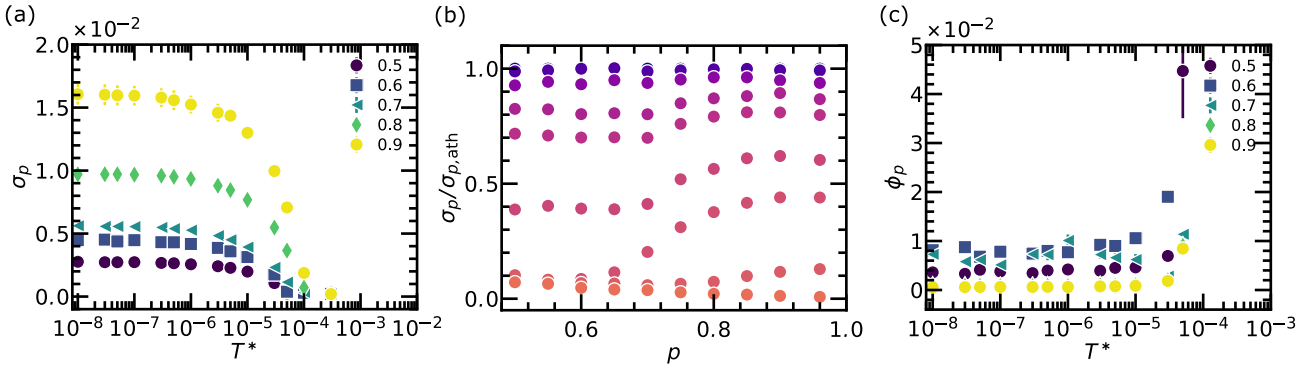

Fig. S9: Main results based on the virial stress σ_{yy} for simulations with $\tau_{\mathrm{break}} = 0.001\ \tau$. Every data point is based on simulations of 10 independent configurations. (a) Peak stress σ_p as a function of the reduced temperature for a range of p (see legend). (b) Connectivity dependence of σ_p normalized by the peak stress in the athermal limit $\sigma_{p,\mathrm{ath}}$ for several reduced temperatures (see legend). (c) Fraction of broken bonds at the peak strain ϕ_p (including the peak event) as a function of T^* for a range of dilution factors $p = 0.50 - 0.90$ (see legend). Fractions are calculated with respect to the initial number of bonds in the diluted network.